

Report Title: "Synthesis and characterization of advanced magnetic materials" for the grant entitled "Laser processing of advanced magnetic materials"

Type of Report: Final

Reporting Period Start Date: September 12, 2002

Reporting Period End Date: September 11, 2004

Principal Author: Professor Monica Sorescu

Date Report was Issued: September 22, 2004

DOE Award Number: DE-FC26-02NT41595

Name and Address of Submitting Organization: Duquesne University, Bayer School of Natural and Environmental Sciences, Department of Physics, Pittsburgh, PA 15282-0321

## DISCLAIMER

This report was prepared as an account of work sponsored by an agency of the United States Government. Neither the United States Government nor an agency thereof, nor any of their employees, makes any warranty, express or implied, or assumes any legal liability or responsibility for the accuracy, completeness, or usefulness of any information, apparatus, product, or process disclosed, or represents that its use would not infringe privately owned rights. Reference herein to any specific commercial product, process, or service by trade name, trademark, manufacturer, or otherwise does not necessarily constitute or imply its endorsement, recommendation, or favoring by the United States Government or any agency thereof. The views and opinions of authors expressed herein do not necessarily reflect those of the United States Government or any agency thereof.

## ABSTRACT

The work described in this grant report was focused mainly on the properties of novel magnetic intermetallics. In the first project, we synthesized several 2:17 intermetallic compounds, namely  $\text{Nd}_2\text{Fe}_{15}\text{Si}_2$ ,  $\text{Nd}_2\text{Fe}_{15}\text{Al}_2$ ,  $\text{Nd}_2\text{Fe}_{15}\text{SiAl}$  and  $\text{Nd}_2\text{Fe}_{15}\text{SiMn}$ , as well as several 1:12 intermetallic compounds, such as  $\text{NdFe}_{10}\text{Si}_2$ ,  $\text{NdFe}_{10}\text{Al}_2$ ,  $\text{NdFe}_{10}\text{SiAl}$  and  $\text{NdFe}_{10}\text{MnAl}$ . In the second project, seven compositions of  $\text{Nd}_x\text{Fe}_{100-x-y}\text{B}_y$  ribbons were prepared by a melt spinning method with Nd and B content increasing from 7.3 and 3.6 to 11 and 6, respectively. The alloys were annealed under optimized conditions to obtain a composite material consisting of the hard magnetic  $\text{Nd}_2\text{Fe}_{14}\text{B}$  and soft magnetic  $\alpha\text{-Fe}$  phases, typical of a spring magnet structure. In the third project, intermetallic compounds of the type  $\text{Zr}_1\text{Cr}_1\text{Fe}_1\text{T}_{0.8}$  with  $\text{T}=\text{Al}$ ,  $\text{Co}$  and  $\text{Fe}$  were subjected to hydrogenation. In the fourth project, we performed three crucial experiments. In the first experiment, we subjected a mixture of  $\text{Fe}_3\text{O}_4$  and  $\text{Fe}$  (80-20 wt %) to mechanochemical activation by high-energy ball milling, for time periods ranging from 0.5 to 14 hours. In the second experiment, we ball-milled  $\text{Fe}_3\text{O}_4\text{:Co}^{2+}$  ( $x=0.1$ ) for time intervals between 2.5 and 17.5 hours. Finally, we exposed a mixture of  $\text{Fe}_3\text{O}_4$  and  $\text{Co}$  (80-20 wt %) to mechanochemical activation for time periods ranging from 0.5 to 10 hours. In all cases, the structural and magnetic properties of the systems involved were elucidated by X-ray diffraction (XRD), Mössbauer spectroscopy and hysteresis loop measurements. The four projects resulted in four papers, which were published in *Intermetallics*, *IEEE Transactions on Magnetics*, *Journal of Materials Science Letters* and *Materials Chemistry and Physics*. The contributions reveal for the first time in literature the effect of substitutions on the hyperfine magnetic field of neodymium-based intermetallics, the correlation between structure and magnetic properties in spring magnets, the unique effects induced by hydrogenation on the hyperfine parameters of iron-rich intermetallics and the characteristics of the ball milling process in systems containing

magnetite.

In a different project, nanostructured magnetite/T multilayers, with T = Ni, Co, Cr, have been prepared by pulsed laser deposition. The thickness of individual magnetite and metal layers takes values in the range of 5 - 40 nm with a total multilayer thickness of 100 -120 nm. X-ray diffraction has been used to study the phase characteristics as a function of thermal treatment up to 550 °C. Small amounts of maghemite and hematite were identified together with prevailing magnetite phase after treatments at different temperatures. The mean grain size of magnetite phase increases with temperature from 12 nm at room temperature to 54 nm at 550 °C. The thermal behavior of magnetite in multilayers in comparison with powder magnetite is discussed. These findings were published in peer-reviewed conference proceedings after presentation at an international materials conference.

Within the frames of another project, structural and morphological characteristics of  $(1-x)\alpha\text{-Fe}_2\text{O}_3\text{-}x\text{SnO}_2$  ( $x=0.0\text{-}1.0$ ) nanoparticles obtained under hydrothermal conditions have been investigated by X-ray diffraction (XRD), transmission Mössbauer spectroscopy, scanning (SEM) and transmission electron microscopy (TEM) as well as energy dispersive X-ray analysis (EDX) [1-13]. On the basis of the Rietveld structure refinements of the XRD spectra at low tin concentrations, it was found that  $\text{Sn}^{4+}$  ions partially substitute for  $\text{Fe}^{3+}$  at the octahedral sites and also occupy the interstitial octahedral sites which are vacant in  $\alpha\text{-Fe}_2\text{O}_3$  corundum structure. A phase separation of  $\alpha\text{-Fe}_2\text{O}_3$  and  $\text{SnO}_2$  was observed for  $x \geq 0.4$ : the  $\alpha\text{-Fe}_2\text{O}_3$  structure containing tin decreases simultaneously with the increase of the  $\text{SnO}_2$  phase containing substitutional iron ions. The mean particle dimension decreases from 70 nm to 6 nm, as the molar fraction  $x$  increases up to  $x=1.0$ . The estimated solubility limits in the nanoparticle system  $(1-x)\alpha\text{-Fe}_2\text{O}_3\text{-}x\text{SnO}_2$  synthesized under hydrothermal conditions are:  $x \leq 0.2$  for  $\text{Sn}^{4+}$  in  $\alpha\text{-Fe}_2\text{O}_3$  and  $x \geq 0.7$  for  $\text{Fe}^{3+}$  in  $\text{SnO}_2$ . These findings were published in the Journal of Physics and Chemistry of Solids.

Tin-doped hematite nanoparticles  $(1-x)\alpha\text{-Fe}_2\text{O}_3\text{-}x\text{SnO}_2$  were synthesized again using the hydrothermal method. The samples were characterized using Mössbauer spectroscopy as a function of the substitution level  $x$ . The recoilless fraction was determined using the dual absorber method introduced by us [M. Sorescu, Mater. Lett. 54 (2002) 256]. It has been observed that the recoilless fraction of the hematite samples first decreases with increasing the amount  $x$  of tin substitution, then increases as iron enters the  $\text{SnO}_2$  lattice and finally, it slightly decreases again as the particle size of the nanoparticles decreases.

In a related work,  $\alpha\text{-Fe}_2\text{O}_3\text{-In}_2\text{O}_3$  mixed oxide nanoparticles system has been synthesized by hydrothermal supercritical and postannealing route, starting with  $(1-x)\text{Fe}(\text{NO}_3)_3\cdot 9\text{H}_2\text{O}\cdot x\text{In}(\text{NO}_3)_3\cdot 5\text{H}_2\text{O}$  aqueous solution ( $x=0\text{-}1$ ). X-ray diffraction and Mössbauer spectroscopy have been used to study the phase structure and substitutions in the nanosized samples [14-34]. The concentration regions for the existence of the solid-solutions in the  $\alpha\text{-Fe}_2\text{O}_3\text{-In}_2\text{O}_3$  nanoparticle system together with the solubility limits of  $\text{In}^{3+}$  ions in the hematite lattice and of  $\text{Fe}^{3+}$  ions in the cubic  $\text{In}_2\text{O}_3$  structure have been evidenced. In general, the substitution level is considerably lower than the nominal concentration  $x$ . A justification of the processes leading to the formation of iron and indium phases in the investigated supercritical hydrothermal system has been given.

In a different project we proposed to study the structural and magnetic properties of  $\alpha\text{-Fe/Nd}_2\text{Fe}_{14}\text{B}$  magnetic multilayers obtained by pulsed laser deposition (PLD) [35-43]. The  $\alpha\text{-Fe}$  and  $\text{Nd}_2\text{Fe}_{14}\text{B}$  sputtering targets were obtained from Goodfellow Corporation. The PLD process was conducted with a KrF excimer laser having a wavelength of 248 nm and a pulse width of 8 ns. The laser delivered 450 mJ/pulse at a repetition rate of 10 Hz. For each laser pulse, a fluence at target of about  $3\text{ J/cm}^2$  was obtained. The multilayered films were deposited on (100) Si

wafers, then measured and subsequently annealed before new measurements were performed.

Spring magnets of the type  $\alpha$ -Fe/Nd<sub>2</sub>Fe<sub>14</sub>B consist of a soft phase ( $\alpha$ -Fe) and a hard phase (Nd<sub>2</sub>Fe<sub>14</sub>B), which are exchange coupled. These nanocomposite magnetic materials exhibit high magnetic remanence, high coercivity, high energy product and low cost [44-54]. In these nanostructures, the enhancement of magnetic properties is related to the exchange coupling between hard and soft nanograins. In the final project we proposed to study the effect of Co substitutions on the structural and magnetic properties of spring magnets. We employed X-ray diffraction (XRD) and Mössbauer spectroscopy to characterize the main features of Co additions and in particular, to answer the question of whether Co enters the soft phase or the hard phase. Three compositions of spring magnets, Nd<sub>11</sub>Fe<sub>80.6</sub>Co<sub>2.6</sub>B<sub>5.8</sub>, Nd<sub>10.5</sub>Fe<sub>78.4</sub>Co<sub>5.3</sub>B<sub>5.8</sub> and Nd<sub>10</sub>Fe<sub>76.5</sub>Co<sub>7.9</sub>B<sub>5.6</sub> were prepared by arc melting and annealed for 3 min at 690, 720, 755 and 775°C.

Consequently, this grant deals with several synthetic methods to obtain advanced magnetic materials (hydrothermal method, mechanochemical synthesis and laser ablation) and several characterization techniques, such as X-ray diffraction, Mössbauer spectroscopy, magnetometry and electron microscopy.

## TABLE OF CONTENTS

Title page	1
Disclaimer	2
Abstract	3
List of graphical materials	8
Introduction	9
Executive summary	12
Experimental	14
Results and discussion	17
Conclusion	30
References	32
List of acronyms and abbreviations	35
List of publications	36

## LIST OF GRAPHICAL MATERIAL

FIG. 1. Recoilless fraction of the tin-doped hematite nanoparticle system as function of the amount  $x$  of tin substitution.

FIG. 2. Phase balance in the supercritical hydrothermal samples after the thermal treatment at 500 °C for one hour, as resulted from XRD spectra. Phase index: (●)  $H_x$ , isostructural with  $\alpha$ - $Fe_2O_3$ ; (○)  $B_x$ , isostructural with cubic phase  $In_2O_3$ .

FIG. 3. Conversion electron Mössbauer spectra of the  $\alpha$ -Fe/ $Nd_2Fe_{14}B$  multilayers obtained for an ablation time of (a) 15 min; (b) 30 min and (c) 60 min for each target. In (A)-(C) the hyperfine magnetic field distributions extracted from the CEMS spectra are given.

FIG. 4. Room temperature transmission Mössbauer spectra of  $Nd_{11}Fe_{80.6}Co_{2.6}B_{5.8}$  after annealing at (a) 690 and (b) 755°C. In Fig. 2 (A) and (B) the corresponding hyperfine magnetic field distributions are given.



## INTRODUCTION

The introductory statements for intermetallics were presented in previous reports.

Due to their sensing properties in detection of dangerous gases, much attention has been devoted recently to the study of semiconducting oxides. Enhanced gas sensing properties are associated with nanostructured semiconductive oxides, due to their high surface areas and activities. The nanostructured oxide system  $(1-x)\alpha\text{-Fe}_2\text{O}_3\text{-}x\text{SnO}_2$  has been synthesized by various methods, especially at low tin content.

Most recently, we investigated the structural, magnetic and morphological characteristics of  $(1-x)\alpha\text{-Fe}_2\text{O}_3\text{-}x\text{SnO}_2$  nanoparticles obtained by hydrothermal synthesis using X-ray diffraction, Mössbauer spectroscopy, scanning and transmission electron microscopy as well as energy dispersive X-ray analysis. We found that  $\text{Sn}^{4+}$  ions partially substitute for  $\text{Fe}^{3+}$  at the octahedral sites. For  $x \geq 0.4$ , a phase separation of  $\alpha\text{-Fe}_2\text{O}_3$  and  $\text{SnO}_2$  was observed.

However, there is still persisting controversy on the site preference of substitutions in this system. One way to overcome this difficulty is to follow the variation of the Mössbauer recoilless fraction  $f$  of the  $(1-x)\alpha\text{-Fe}_2\text{O}_3\text{-}x\text{SnO}_2$  system as function of the substitution level  $x$ .

The classical method for determination of the recoilless fraction is believed to be inaccurate, due to the large errors associated with the determination of the Debye temperature. Recently, we proposed a new method for the direct determination of the recoilless fraction using a single room-temperature Mössbauer measurement of a two-foil absorber. In this work we applied the dual absorber method to obtain the recoilless fraction of the tin-doped hematite nanoparticles as function of the substitution level  $x$ . The results are correlated with the lattice occupancy of the Fe atoms.

Owing to their potential uses in micro and optoelectronics or as sensing materials, the

fabrication of nanosized oxides has attracted significant interest in the last decade. A large number of oxides such as  $\text{SnO}_2$ ,  $\text{In}_2\text{O}_3$ ,  $\text{TiO}_2$ ,  $\text{Fe}_2\text{O}_3$ , and mixed oxides were reported to be sensitive to certain gas species. In particular, improved sensing properties have been obtained in the mixed system indium oxide-alpha iron oxide.

Indium oxide has two crystalline structures: the cubic lattice, known as bixbyite structure and the rhombohedral or corundum structure. The cubic  $\text{In}_2\text{O}_3$  phase, in powder form, has been prepared by different methods such as chemical coprecipitation followed by annealing and calcination. The corundum structure  $\text{In}_2\text{O}_3$  is a high pressure modification of indium oxide, which implies difficulties in the experimental steps and consequently has been hardly ever produced. In a previous paper we reported on the possibility to obtain the corundum structure  $\text{In}_2\text{O}_3$  by a hydrothermal and post annealing route, at moderate temperatures and pressures (200 °C and 15 atm).

The corundum structure of  $\alpha\text{-Fe}_2\text{O}_3$  (hematite) is based on hexagonal close packing of oxygen with iron in 2/3 of the octahedral vacancies. At room temperature hematite is a weak ferromagnet. The preparation methods of hematite include solid phase reaction of iron hydroxides, chemical wet methods and the hydrothermal method.

$\text{In}_2\text{O}_3$  and  $\text{Fe}_2\text{O}_3$  exhibit only a partial solid solubility at atmospheric pressure. In the system  $\text{In}_{2-y}\text{Fe}_y\text{O}_3$ , the bixbyite cubic structure of  $\text{In}_2\text{O}_3$  occurs in the concentration range  $0 \leq y < 0.87$  and the corundum structure at values of  $y$  only slightly less than 2. Nevertheless, at elevated pressure the system forms a complete solid solution series having the corundum structure. In the  $\alpha\text{-Fe}_2\text{O}_3\text{--In}_2\text{O}_3$  system prepared by coprecipitation followed by annealing it was found that indium and iron substituted oxide phases,  $(\text{Fe}_{1-x}\text{In}_x)_2\text{O}_3$ , isostructural with  $\alpha\text{-Fe}_2\text{O}_3$  or cubic  $\text{In}_2\text{O}_3$  are present in a wide indium concentration range. However, the solid solution in the  $\text{Fe}_2\text{O}_3\text{--In}_2\text{O}_3$  system occurs in narrow concentration regions at iron-rich area and at indium-rich

area (limited at  $x=0.1$  for Indium in  $\alpha\text{-Fe}_2\text{O}_3$  and from  $x=0.8$  to  $x=1.0$ , for Iron in  $\text{In}_2\text{O}_3$ ). In the  $(\text{In}_{1-z}\text{Fe}_z)_2\text{O}_3$  samples obtained at  $1500^\circ\text{C}$  in air the solubility of  $\text{Fe}_2\text{O}_3$  in  $\text{In}_2\text{O}_3$  was found to be limited at  $z=0.33$ .

With the goal to obtain the mixed oxide  $\alpha\text{-Fe}_2\text{O}_3\text{--In}_2\text{O}_3$  particle system, at nanometric scale in an extended solubility range, this paper is aimed at studying the behavior of  $(1-x)\text{Fe}(\text{NO}_3)_3 \cdot 9\text{H}_2\text{O} \cdot x\text{In}(\text{NO}_3)_3 \cdot 5\text{H}_2\text{O}$  water solution ( $x=0.0\text{--}1.0$ ), under supercritical conditions. X-ray diffraction (XRD) on powder as well as the Mössbauer transmission spectroscopy methods have been used to investigate the supercritical hydrothermal reaction products. Indium substituted hematites and Iron substituted cubic indium oxide together with a small amount of  $\text{InOOH}$  are formed in the supercritical hydrothermal system. By annealing, the  $\text{InOOH}$  phase dehydrates to bixbyite indium oxide. The solubility of indium in the hematite phase and respectively of iron in the bixbyite structure are evidenced and discussed. The oxide phase crystallization under hydrothermal conditions is explained in terms of hydrolysis processes.

Spring magnets of the type  $\alpha\text{-Fe/Nd}_2\text{Fe}_{14}\text{B}$  consist of a soft ( $\alpha\text{-Fe}$ ) magnetic phase embedded into a hard ( $\text{Nd}_2\text{Fe}_{14}\text{B}$ ) magnetic phase, which results in a high remanent polarization provided that the particles are small and strongly exchanged coupled. This type of structure can also be obtained through a multilayered two-phase magnet, consisting of thin alternating soft and hard magnetic layers. These  $\alpha\text{-Fe/Nd}_2\text{Fe}_{14}\text{B}$  nanocomposite magnetic materials exhibit high magnetic remanence, high coercivity, high energy product and low cost. In these nanostructures, the enhancement of magnetic properties is related to the exchange coupling between hard and soft nanograins. In this project we propose to study the effect of Co substitutions on the structural and magnetic properties of spring magnets. We employ X-ray diffraction (XRD) and Mössbauer spectroscopy to characterize the main features of Co additions and in particular, to answer the question of whether Co enters the soft phase or the hard phase.

## EXECUTIVE SUMMARY

In the first project, we synthesized several 2:17 intermetallic compounds, namely  $\text{Nd}_2\text{Fe}_{15}\text{Si}_2$ ,  $\text{Nd}_2\text{Fe}_{15}\text{Al}_2$ ,  $\text{Nd}_2\text{Fe}_{15}\text{SiAl}$  and  $\text{Nd}_2\text{Fe}_{15}\text{SiMn}$ , as well as several 1:12 intermetallic compounds, such as  $\text{NdFe}_{10}\text{Si}_2$ ,  $\text{NdFe}_{10}\text{Al}_2$ ,  $\text{NdFe}_{10}\text{SiAl}$  and  $\text{NdFe}_{10}\text{MnAl}$ . The substitutional effect on their magnetic properties was studied by Mössbauer spectroscopy using hyperfine magnetic field distributions. The structural properties of both classes of intermetallics were investigated using XRD. For both symmetries involved, it was found that Al and especially, Mn substitutions lower the value of the net magnetic moment, while Si additions correlate with high values of the average magnetic field and consequently, magnetic moment.

In the second project, seven compositions of  $\text{Nd}_x\text{Fe}_{100-x-y}\text{B}_y$  ribbons were prepared by a melt spinning method, with Nd and B content increasing from 7.3 and 3.6 to 11 and 6, respectively. The alloys were annealed under optimized conditions to obtain a composite material consisting of the hard magnetic  $\text{Nd}_2\text{Fe}_{14}\text{B}$  and soft magnetic  $\alpha\text{-Fe}$  phases, typical of a spring magnet structure. Phase analysis was performed by X-ray diffraction and Mössbauer spectroscopy, in order to obtain the hyperfine magnetic fields and site populations. In all alloys, the  $\text{Nd}_2\text{Fe}_{14}\text{B}$  and  $\alpha\text{-Fe}$  phases were formed due to annealing. However, in the case of  $\text{Nd}_{11}\text{Fe}_{83}\text{B}_6$  alloy with the highest Nd content a significant amount of the  $\text{Nd}_{11}\text{Fe}_4\text{B}_4$  paramagnetic phase was observed. In the studied set of alloys, the highest fraction of the  $\alpha\text{-Fe}$  phase (about 30 %) was obtained for the  $\text{Nd}_{7.3}\text{Fe}_{89.1}\text{B}_{3.6}$  alloy. The formation of the exchange coupled material was checked by hysteresis loop measurements at room temperature in all cases.

In the third project, intermetallic compounds of the type  $\text{Zr}_1\text{Cr}_1\text{Fe}_1\text{T}_{0.8}$  with  $\text{T}=\text{Al}$ ,  $\text{Co}$  and  $\text{Fe}$  were subjected to hydrogenation. The structural and magnetic properties of these intermetallic compounds and their hydrides were studied by Mössbauer spectroscopy at room and liquid helium temperatures. The effects observed to be induced by hydrogenation ranged from changes in site populations and onset of crystallographic disorder to enhancement of weak ferromagnetism in the compound with  $\text{Fe}$ .

In the fourth project, we performed three crucial experiments. In the first experiment, we subjected a mixture of  $\text{Fe}_3\text{O}_4$  and  $\text{Fe}$  (80-20 wt %) to mechanochemical activation by high-energy ball milling, for time periods ranging from 0.5 to 14 hours. Complementary XRD and Mössbauer spectroscopy data demonstrated a phase transformation of magnetite to hematite, accompanied by a partial oxidation of iron to hematite. The reaction can be used to obtain nanometer-size magnetite by ball milling, due to the inhibition of its transformation to hematite, caused by the presence of iron atoms. In the second experiment, we ball-milled  $\text{Fe}_3\text{O}_4\text{:Co}^{2+}$  ( $x=0.1$ ) for time intervals between 2.5 and 17.5 hours. Our XRD and Mössbauer measurements showed that the cobalt-doped magnetite undergoes a phase transformation to hematite, which is actually cobalt-doped hematite. We were able to show herewith that the Co ion is not kicked out of the lattice during the milling process, but undergoes the phase transformation inside the hematite lattice. Finally, we exposed a mixture of  $\text{Fe}_3\text{O}_4$  and  $\text{Co}$  (80-20 wt %) to mechanochemical activation for time periods ranging from 0.5 to 10 hours. The XRD and Mössbauer results are consistent with the formation of cobalt ferrite (a strongly Co-substituted magnetite), with the occurrence of hematite as an intermediate product. In all three cases, the milling-induced phase transformations started with a considerable disorder of the octahedral sublattice of magnetite.

The four projects summarized here resulted in four papers, which were published in *Intermetallics*, *IEEE Transactions on Magnetics*, *Journal of Materials Science Letters* and *Materials Chemistry and Physics*.

An alternate project proposes and achieves the laser ablation deposition of  $\text{Fe}_3\text{O}_4/\text{T}$

multilayers, with T=Ni, Cr and Co. The total thickness of the multilayers was about 100 nm, with individual layer thickness in the range 5-40 nm. The multilayers were subjected to postdeposition annealing at temperatures up to 550°C. We used X-ray diffraction in order to characterize the phase characteristics as a function of thermal treatment. The average grain size of magnetite phase was found to increase from 12 nm at room temperature to 54 nm at 550°C. Finally, we provide a direct comparison between the thermal behavior of magnetite in multilayers and that of bulk magnetite.

The next work proposes and achieves the hydrothermal synthesis of  $(1-x)\alpha\text{-Fe}_2\text{O}_3\text{-}x\text{SnO}_2$  ( $x=0.0\text{-}1.0$ ) nanoparticles. The system has been investigated by X-ray diffraction (XRD), transmission Mössbauer spectroscopy, scanning (SEM) and transmission electron microscopy (TEM) as well as energy dispersive X-ray analysis (EDX). Based on the Rietveld structure refinements of the XRD spectra at low tin concentrations, it was found that  $\text{Sn}^{4+}$  ions partially substitute for  $\text{Fe}^{3+}$  at the octahedral sites and also occupy the interstitial octahedral sites which are vacant in  $\alpha\text{-Fe}_2\text{O}_3$  corundum structure. For  $x \geq 0.4$ , a phase separation of  $\alpha\text{-Fe}_2\text{O}_3$  and  $\text{SnO}_2$  was observed: the  $\alpha\text{-Fe}_2\text{O}_3$  structure containing tin decreases simultaneously with the increase of the  $\text{SnO}_2$  phase containing substitutional iron ions. As determined from TEM, the mean particle dimension decreases from 70 nm to 6 nm, as the molar fraction  $x$  increases up to  $x=1.0$ . The recoilless fraction was determined using the dual absorber method introduced by us [M. Sorescu, Mater. Lett. 54 (2002) 256]. It has been observed that the recoilless fraction of the hematite samples first decreases with increasing the amount  $x$  of tin substitution, then increases as iron enters the  $\text{SnO}_2$  lattice and finally, it slightly decreases again as the particle size of the nanoparticles decreases.

$\alpha\text{-Fe}_2\text{O}_3\text{-In}_2\text{O}_3$  mixed oxide nanoparticles system has been synthesized by hydrothermal supercritical and postannealing route, starting with  $(1-x)\text{Fe}(\text{NO}_3)_3 \cdot 9\text{H}_2\text{O} \cdot x\text{In}(\text{NO}_3)_3 \cdot 5\text{H}_2\text{O}$  aqueous solution ( $x=0\text{-}1$ ). X-ray diffraction and Mössbauer spectroscopy have been used to study the phase structure and substitutions in the nanosized samples. The concentration regions for the existence of the solid-solutions in the  $\alpha\text{-Fe}_2\text{O}_3\text{-In}_2\text{O}_3$  nanoparticle system together with the solubility limits of  $\text{In}^{3+}$  ions in the hematite lattice and of  $\text{Fe}^{3+}$  ions in the cubic  $\text{In}_2\text{O}_3$  structure have been evidenced. In general, the substitution level is considerably lower than the nominal concentration  $x$ . A justification of the processes leading to the formation of iron and indium phases in the investigated supercritical hydrothermal system has been given.

We proposed to study the structural and magnetic properties of  $\alpha\text{-Fe/Nd}_2\text{Fe}_{14}\text{B}$  magnetic multilayers obtained by pulsed laser deposition (PLD). We employed X-ray diffraction (XRD) and conversion electron Mössbauer spectroscopy (CEMS) to characterize the main features of the  $\alpha\text{-Fe/Nd}_2\text{Fe}_{14}\text{B}$  multilayer systems. In this work we also proposed to study the effect of Co substitutions on the structural and magnetic properties of spring magnets. We employed X-ray diffraction (XRD) and Mössbauer spectroscopy to characterize the main features of Co additions and in particular, to answer the question of whether Co enters the soft phase or the hard phase.

## EXPERIMENTAL

Experimental details for the intermetallics were given in a previous report.

Hydrothermal synthesis of the system  $(1-x)\alpha\text{-Fe}_2\text{O}_3\text{-}x\text{SnO}_2$  ( $x=0.0\text{-}1.0$ ) was performed in a 50 mL stainless steel autoclave, starting with an aqueous mixture of iron (III) chloride hexahydrate,  $\text{FeCl}_3\cdot 6\text{H}_2\text{O}$  and of tin (IV) chloride pentahydrate,  $\text{SnCl}_4\cdot 5\text{H}_2\text{O}$ . A 25% ammonium hydroxide solution was used as precipitation agent to attain a pH equal to 8. The suspension was heated in autoclave at  $200^\circ\text{C}$  for 4 hours and then quenched to room temperature. The corresponding vapor pressure at  $200^\circ\text{C}$  was about 15 atm. The resulted precipitate was filtered, washed with water until no chloride ions were detected by silver nitrate solution and then dried in a furnace at  $105^\circ\text{C}$ .

Room temperature transmission Mössbauer spectra were recorded using a  $^{57}\text{Co(Rh)}$  source and an MS-1200 constant acceleration spectrometer. The absorbers consisted of a sandwich between the  $(1-x)\alpha\text{-Fe}_2\text{O}_3\text{-}x\text{SnO}_2$  powder and the natural iron etalon foil, with equal masses. All spectra were analyzed by least squares fitting using the NORMOS program.

A series of  $\alpha\text{-Fe}_2\text{O}_3\text{-In}_2\text{O}_3$  samples were prepared under hydrothermal supercritical conditions. The syntheses were performed in a stainless steel high pressure cell starting with  $(1-x)\text{Fe}(\text{NO}_3)_3\cdot 9\text{H}_2\text{O}\cdot x\text{In}(\text{NO}_3)_3\cdot 5\text{H}_2\text{O}$  aqueous solution ( $x=0\text{-}1$ ). The reaction cell is a stainless steel cylinder of 220 mm length, 25 mm diameter and a corresponding inner volume of about 24 mL. The temperature control was assured by a proportional controller with an accuracy of  $\pm 2^\circ\text{C}$ , by using a chromel-alumel thermocouple. In all experiments the filling factor was 0.5. The precursors used in the hydrothermal syntheses were iron (III) nitrate nanohydrate (Merck, analytical grade reagent) and indium (III) nitrate pentahydrate (Aldrich, 99.99%). Corresponding amounts of both nitrates were separately dissolved in distilled water. The

aqueous solutions were mixed by adding the iron nitrate solution to the indium nitrate solution, then introduced into the reaction cell, heated up to 400°C with a heating rate of 10°C/min. and kept at this temperature for 4 hours. The corresponding pressure was 300 MPa. In all experiments the total nitrate concentration of the final solution was 0.5 M. After cooling to room temperature, the resulted precipitate was washed with distilled water and separated by centrifugal method. The incorporated water was removed with acetone and finally, the reaction product was dried at 50°C in air. Owing to the nature of the synthesis process, the accurate substitution level could not be consistently predicted and  $x$  values represent the nominal indium molar concentrations.

The structure of as-resulted powders was examined with a Rigaku D-2013 X-ray diffractometer using  $\text{CuK}_\alpha$  radiation ( $\lambda = 1.540598 \text{ \AA}$ ). The  $^{57}\text{Fe}$  Mössbauer spectra were recorded at room temperature using a source of  $^{57}\text{Co}$  in Rh matrix and an MS-1200 constant acceleration spectrometer. The sample thickness was  $7 \text{ mg Fe/cm}^2$ . The thermal treatments (Rapid temperature furnace, Bloomfield N. J.) were performed in ambient atmosphere, at 500 °C, for one hour. After annealing, the samples were cooled to room temperature and investigated by XRD and Mössbauer spectroscopy.

The  $\alpha\text{-Fe}$  and  $\text{Nd}_2\text{Fe}_{14}\text{B}$  sputtering targets were obtained from Goodfellow Corporation. The PLD process was conducted with a KrF excimer laser having a wavelength of 248 nm and a pulse width of 8 ns. The laser delivered 450 mJ/pulse at a repetition rate of 10 Hz. For each laser pulse, a fluence at target of about  $3 \text{ J/cm}^2$  was obtained. The multilayered films were deposited on (100) Si wafers, then measured and subsequently annealed before new measurements were performed. We employed X-ray diffraction (XRD) and conversion electron Mössbauer spectroscopy (CEMS) to characterize the main features of the  $\alpha\text{-Fe}/\text{Nd}_2\text{Fe}_{14}\text{B}$  multilayer systems. XRD measurements were performed using a Rigaku D-2013 diffractometer

with Cu  $K_{\alpha 1}$  radiation at  $\lambda=1.5404 \text{ \AA}$ . CEMS measurements were made with a constant acceleration spectrometer. The 50 mCi gamma ray source was  $^{57}\text{Co}$  in Rh matrix, maintained at room temperature. A He-6 %  $\text{CH}_4$  gas-flowed electron counter was used. All spectra were analyzed with the NORMOS-DIST program, which uses the histogram method to obtain the hyperfine magnetic field distributions.

Three compositions of spring magnets,  $\text{Nd}_{11}\text{Fe}_{80.6}\text{Co}_{2.6}\text{B}_{5.8}$ ,  $\text{Nd}_{10.5}\text{Fe}_{78.4}\text{Co}_{5.3}\text{B}_{5.8}$  and  $\text{Nd}_{10}\text{Fe}_{76.5}\text{Co}_{7.9}\text{B}_{5.6}$  were prepared by arc melting and annealed for 3 min at 690, 720, 755 and 775°C. XRD measurements were performed using a Rigaku D-2013 diffractometer with Cu  $K_{\alpha 1}$  radiation at  $\lambda=1.5404 \text{ \AA}$ . Transmission Mössbauer measurements were made with a constant acceleration spectrometer. The 50 mCi gamma ray source was  $^{57}\text{Co}$  in Rh matrix, maintained at room temperature. All spectra were analyzed with the NORMOS-DIST program, which uses the histogram method to obtain the hyperfine magnetic field distributions.



## RESULTS AND DISCUSSION

### I. Recoilless fraction of tin-doped hematite nanoparticles

We recorded the room temperature transmission Mössbauer spectra of the  $(1-x)\alpha\text{-Fe}_2\text{O}_3\text{-}x\text{SnO}_2$  system with the natural iron foil, corresponding to values of  $x=0.0, 0.1, 0.2$  and  $0.3$ , respectively. All spectra were analyzed considering two sextets. One sextet corresponds to the iron foil and the other stands for the tin-doped hematite system. The amount of hematite was found to decrease with increasing the amount  $x$  of tin substitution.

We also measured the room temperature transmission Mössbauer spectra of the  $(1-x)\alpha\text{-Fe}_2\text{O}_3\text{-}x\text{SnO}_2$  system with the natural iron foil, corresponding to values of  $x=0.4, 0.5, 0.6, 0.7$  and  $0.8$ , respectively. All spectra were fitted with a sextet, corresponding to the iron foil and a doublet, representing the Fe atoms in the  $\text{SnO}_2$  structure.

As it has been demonstrated by us, the recoilless fraction in a dual absorber experiment can be calculated from the relative areas of the subspectra and the corresponding molar masses, according to the formula  $A_{\text{Fe}}/A_{\text{hem}}=(\mu_{\text{hem}}/\mu_{\text{Fe}})(f_{\text{Fe}}/f_{\text{hem}})$ . The values obtained for  $f_{\text{hem}}$  are plotted in Figure 1 as function of the substitution level  $x$ . It can be seen that the recoilless fraction of the  $(1-x)\alpha\text{-Fe}_2\text{O}_3\text{-}x\text{SnO}_2$  system decreases from 0.76 to 0.12 for  $x\leq 0.4$ , due to tin substituting iron in the hematite structure. For  $0.4\leq x\leq 0.6$  the recoilless fraction increases from 0.12 to 0.28, due to iron substituting tin in the  $\text{SnO}_2$  lattice. Moreover, the recoilless fraction of the nanoparticle system decreases again from 0.28 to 0.2 for  $0.6\leq x\leq 0.8$ , as effect of the reduction of particle size in the structure [9].

Consequently, this study on the recoilless fraction of the tin-doped hematite nanoparticle system supports the substitutional model as opposed to interstitial occupancy of sites in this structure.

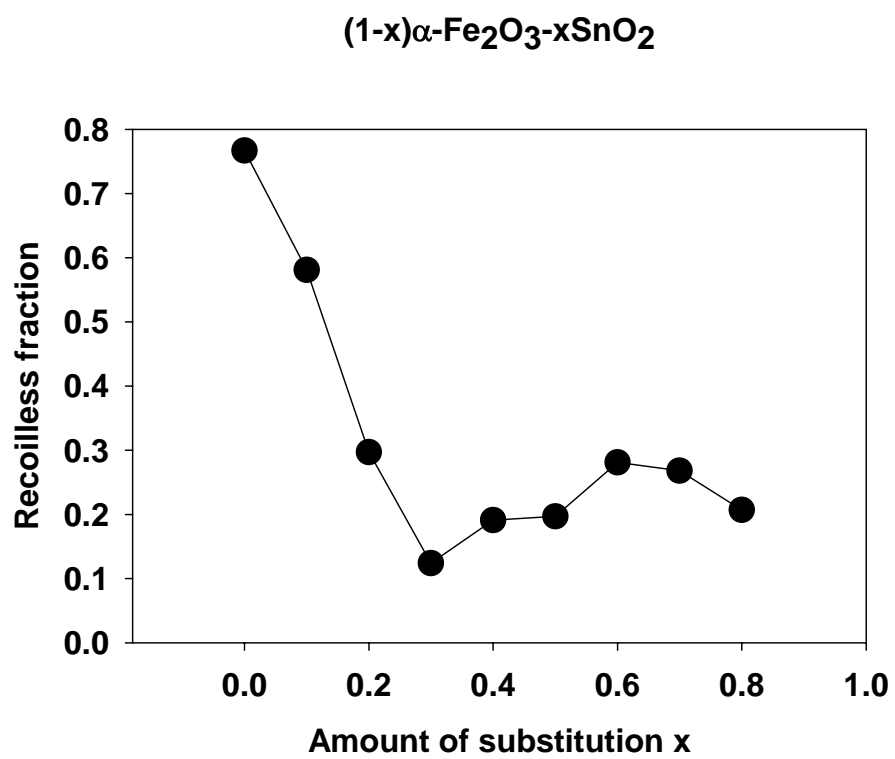


Figure 1

## II. Hematite-indium oxide mixed nanoparticles

The X-ray diffraction patterns of the supercritical hydrothermal samples have been analyzed to study the phase structure in relation with indium concentration  $x$  in the system. XRD spectra from all concentration range were recorded. At  $x=0$  the XRD spectrum corresponds to pure  $\alpha$ -Fe<sub>2</sub>O<sub>3</sub> (Inorganic Crystal Structure Database (ICSD), code 15840, S.G. 167, R32/c) synthesized under hydrothermal supercritical conditions from Fe(NO<sub>3</sub>)<sub>3</sub>·9H<sub>2</sub>O. By increasing indium content in the hydrothermal system, the hematite lines change in both positions and intensities and some other phases can be identified in the XRD spectra. In the following, the modified hematite phases will be named H <sub>$x$</sub>  phases. At  $x=0.1$  the XRD pattern can be indexed with H <sub>$x$</sub>  lines only while at  $x=0.2$  beside the prominent H <sub>$x$</sub>  phase, small peaks corresponding to indium oxyhydroxide, InOOH (ICSD code 24093, S.G. 58, Pnnm) can be observed. Bixbyite-like cubic structure (B <sub>$x$</sub>  in what follows) of In<sub>2</sub>O<sub>3</sub> (ICSD code 14388, S.G. 206, Ia3) appears at  $x=0.3$  in extend of approximately 2% together with InOOH and still prevailing hematite-like phase. At higher indium molar concentrations, a decrease of H <sub>$x$</sub>  phase accompanied by an increase of indium oxide, B <sub>$x$</sub>  phase was observed. The relative abundance of InOOH is about 8-11%. In the concentration range  $x=0.8$ - $0.9$  the dominant component in the XRD pattern is the B <sub>$x$</sub>  phase, but the H <sub>$x$</sub>  phase and indium oxihydroxide still exist in significant amounts. At  $x=1$  the prevailing component in the XRD spectrum, cubic In<sub>2</sub>O<sub>3</sub>, is still accompanied by indium oxyhydroxide phase. The transformation into bixbyite phase is not completed at 4 hours of supercritical hydrothermal treatment. The same degree of transformation was also found for longer treatment times (up to 8 hours).

The refinement of XRD spectra indicates an increase of lattice parameters  $a$  and  $c$  of the  $\alpha$ -Fe<sub>2</sub>O<sub>3</sub> structure as the Indium molar content  $x$  increases up to  $x\approx 0.7$  in the hydrothermal system. Since the radius of In<sup>3+</sup> ion is greater ( $\approx 0.94$  Å) than the radius of Fe<sup>3+</sup> ion ( $\approx 0.79$  Å),

this behavior is an argument for the dissolution of indium ions in the hematite lattice. The  $^{57}\text{Fe}$  Mössbauer spectra were recorded at room temperature on the samples with  $x=0.1$ ,  $0.5$  and  $0.7$ . In agreement with XRD results, the six line Mössbauer pattern observed belongs to hematite like structure. The observed increase in the line width accompanied by the lowering of the magnetic hyperfine fields, as the indium content  $x$  increases, suggests the presence of  $\text{In}^{3+}$  in the hematite lattice. The best fit of the spectra was obtained by using a distribution of magnetic hyperfine fields caused by the substitution of  $\text{Fe}^{3+}$  by  $\text{In}^{3+}$  ions in the hematite lattice. The probabilities of magnetic hyperfine fields given by the computer fit were derived. The shift of the maximum probability toward smaller values of magnetic hyperfine field together with the increasing broadening of the distributions as the  $x$  values increase, support the hypothesis of indium substituting iron in the hematite lattice. Therefore, a solid solution of the type  $\alpha\text{-(Fe}_{1-x}\text{In}_x)_2\text{O}_3$ ,  $\text{H}_x$ , isostructural with  $\alpha\text{-Fe}_2\text{O}_3$ , develops in the concentration range  $0 < x \leq 0.7$ , in the supercritical hydrothermal system iron nitrate–indium nitrate at  $400\text{ }^\circ\text{C}$ .

A decrease of the bixbyite lattice parameter  $a$ , versus iron concentration  $(1-x)$ , was found in the indium-rich area  $0.7 \leq x < 1$ . Taking into account the ionic radius difference between  $\text{Fe}^{3+}$  and  $\text{In}^{3+}$ , this behavior supports the presence of iron ions in the cubic lattice of  $\text{In}_2\text{O}_3$ . Consequently, one can infer the crystallization of a cubic phase,  $\text{c-(Fe}_{1-x}\text{In}_x)_2\text{O}_3$ ,  $\text{B}_x$ , isostructural with bixbyite structure  $\text{In}_2\text{O}_3$ , in the studied hydrothermal system. XRD analyses reveal the presence of this phase in the concentration range  $0.3 \leq x \leq 1$ . The small increase of the  $\text{In}_2\text{O}_3$  cubic lattice parameter ( $\approx 0.4\%$ ), by decreasing the iron content in the hydrothermal system, suggests a rather limited dissolution of the iron atoms in the bixbyite indium oxide lattice. This behavior is also supported by the Mössbauer spectra of samples at  $x=0.8$  and  $0.9$ , showing only the typical hematite-like sextet.

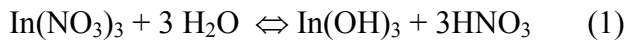
Rietveld structure refinements have been performed in order to obtain information

concerning the site occupancy. In the hematite structure, the  $\text{Fe}^{3+}$  ions with coordinates of (0, 0, z) occupy 2/3 of the octahedral holes in successive oxygen layers, and 1/3 of the octahedral holes with coordinates of (0, 0, 0) is empty. In the case of our samples, the best fit with experimental data has been obtained considering the indium ions only in substitutional (0, 0, z) sites of the hematite corundum type structure. In the cubic indium oxide structure, there are two crystallographically nonequivalent indium atoms sites. No site preference of  $\text{Fe}^{3+}$  substituting  $\text{In}^{3+}$  ions in this phase has been revealed during XRD spectra refinement.

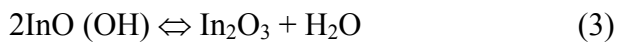
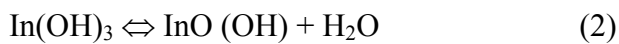
Generally, the substitution degrees resulting from the XRD refinement are sensible lower (up to 40 %) than the nominal concentrations x, the difference coming from the indium or iron phases which are formed simultaneously in the supercritical hydrothermal system. We deduced the phase structure balance in the studied system, as resulted from XRD spectra evaluation. The particle dimensions were determined for hematite and bixbyite phases using the Scherrer equation. For all samples the mean particle dimension belongs to the range of 30-40 nm. A slight decrease, from 40 nm to 30 nm, was evidenced by increasing the indium content x in the hydrothermal system.

A thermal treatment at 500 °C, for 1 hour, was performed for the as resulted supercritical hydrothermal samples. A complete disappearance of  $\text{InOOH}$  phase from the XRD spectra has been observed. This behavior suggests that cubic phase  $\text{In}_2\text{O}_3$  comes from  $\text{InOOH}$  either by hydrothermal processing or by the thermal treatment of hydrothermally crystallized Indium oxyhydroxide. The lattice parameters *a* and *c* of the indium substituted hematite phase versus indium molar concentration x were derived. The increase of lattice parameters as the indium concentration in the system increases supports the presence of indium atoms in the hematite like structure. A phase balance for the samples calcinated at 500 °C for one hour is presented in Figure 2.

We have to remind that both indium oxide and hematite phases obtained under supercritical conditions in the  $(1-x)\text{Fe}(\text{NO}_3)_3 \cdot 9\text{H}_2\text{O} \cdot x\text{In}(\text{NO}_3)_3 \cdot 5\text{H}_2\text{O}$  water solution, for  $x$  values different from 0 and 1, are substituted oxides containing iron and indium ions, respectively. The formation of the iron and indium solid species, identified by XRD spectra analysis, could be explained by the hydrolysis reactions taking place at elevated temperatures in acidic aqueous solutions of the corresponding nitrate mixtures. The hydrolysis equilibria are different for the two metal nitrates. Musić et al. proposed a mechanism for the precipitation of iron oxides or hydroxides by forced hydrolysis of iron (III) salts containing  $\text{Cl}^-$ ,  $\text{NO}_3^-$  or  $\text{SO}_4^{2-}$  anions. The process involves several stages and depends on the nature and concentration of the iron compound, pH, temperature and reaction time. The precipitate formed in iron (III) nitrate solutions at various concentrations was only  $\alpha\text{-Fe}_2\text{O}_3$  phase. In our experiments the nitrate solutions were heated slowly up to 400 °C. In agreement with this mechanism, our XRD results support a complete hydrolysis equilibrium shift toward the formation of hematite. Over the critical point its solubility decreases drastically and it segregates out in the system as precipitate. In the case of indium nitrate solutions, making analogy with the aluminium nitrate solutions behavior under supercritical conditions, we can assume that the reaction equilibrium changes with temperature, leading to the formation of indium hydroxides or oxide. As it was observed in our hydrothermal synthesis experiments, at relatively low temperature ( $\approx 200$  °C), by association of metal cation and hydroxyl anion, the following reaction is possible:



At higher temperatures the dehydration processes become predominant:



As we observed, even after 8 hours of hydrothermal treatment at 400 °C of a 0.5M indium nitrate

solution the equilibrium (3) is not completely shifted to the indium oxide precipitation; both indium solid phases are present and indium oxihydroxide content is still important. The annealing process at 500 °C, for one hour, leads to the dehydration of indium oxihydroxide with the formation of bixbyite phase indium oxide. In the limit of the solubility level at the working temperature,  $\text{In}^{3+}$  ions can substitute  $\text{Fe}^{3+}$  ions in the hematite lattice, up to the nominal concentration  $x=0.7$  of indium nitrate in the hydrothermal system. Moreover, in the nitric acid solutions formed by hydrolysis of the two nitrates, an important part of the precipitated indium compounds redissolves during cooling and they are found again in the solution after the separation of the solid products.

Summarizing, in the series of  $\alpha\text{-Fe}_2\text{O}_3\text{-In}_2\text{O}_3$  nanoparticle samples obtained from the water solution of  $(1-x)\text{Fe}(\text{NO}_3)_3 \cdot 9\text{H}_2\text{O} \cdot x\text{In}(\text{NO}_3)_3 \cdot 5\text{H}_2\text{O}$ , in supercritical hydrothermal conditions, a corundum phase  $\alpha\text{-(Fe}_{1-x}\text{In}_x)_2\text{O}_3$ ,  $\text{H}_x$ , isostructural with  $\alpha\text{-Fe}_2\text{O}_3$  exists for  $0 < x \leq 0.9$  and a cubic phase  $\text{c-(Fe}_{1-x}\text{In}_x)_2\text{O}_3$ ,  $\text{B}_x$ , isostructural with  $\text{In}_2\text{O}_3$  exists for  $0.3 \leq x < 1$ . However, the solubility of  $\text{In}^{3+}$  ions in hematite lattice occurs in the range  $0 < x \leq 0.7$ , while the solubility of  $\text{Fe}^{3+}$  in the bixbyite structure  $\text{In}_2\text{O}_3$  takes place in the range  $0.7 \leq x < 1$ . The substitution level is generally up to 40% lower than indium nominal concentration  $x$ . Consequently, the solid solutions  $\alpha\text{-(Fe}_{1-x}\text{In}_x)_2\text{O}_3$  and  $\text{c-(Fe}_{1-x}\text{In}_x)_2\text{O}_3$ , expand for indium nominal molar concentration  $x$  up to 0.7, and respectively for  $x$  from  $\approx 1.0$  to 0.7, in the studied nanoparticles system. These data are in good agreement with the previous finding, moreover due to supercritical reaction conditions the solubility limits are extended to higher concentration values.

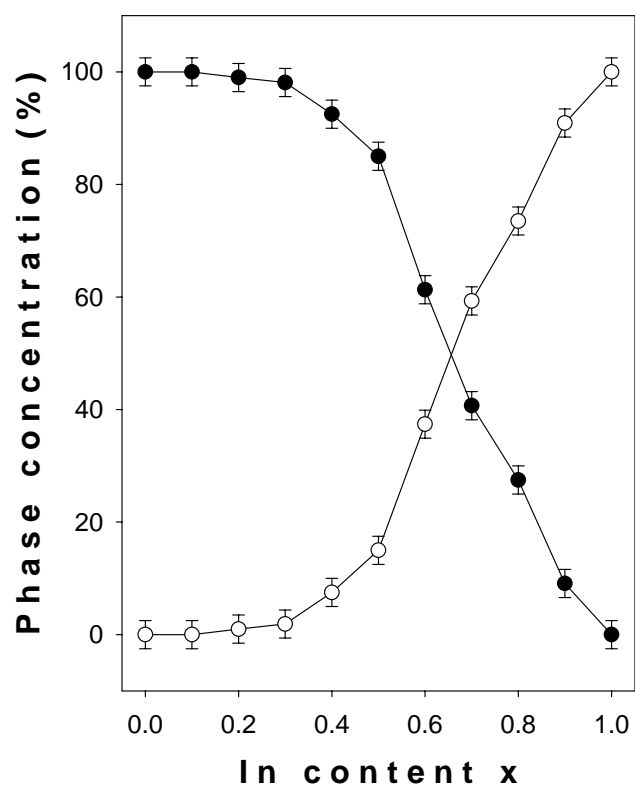


Figure 2



### III. $\alpha$ -Fe/Nd<sub>2</sub>Fe<sub>14</sub>B multilayers

Figure 3 (a)-(c) shows the CEMS spectra of the  $\alpha$ -Fe/Nd<sub>2</sub>Fe<sub>14</sub>B multilayers deposited for 15, 30 and 60 min for each target. In (A)-(C) the hyperfine magnetic field distributions extracted from these spectra are given. The CEMS spectra were analyzed by considering a six-line pattern corresponding to the  $\alpha$ -Fe soft phase and a hyperfine magnetic field distribution, representing the Nd<sub>2</sub>Fe<sub>14</sub>B hard phase. The average values of the distributions were 21.17 and 15.76 T, respectively and the distributions extended over 77.07 and 73.47 % of the spectra in Figure 3 (a)-(b). It may be observed that a decrease in the average hyperfine magnetic field and population of the disordered phase is obtained by employing longer deposition times for each target on the carroussel. Moreover, when we analyze the spectrum in Figure 3 (c), we observe that it consists entirely of a distribution of hyperfine magnetic fields, with an average value of 5.25 T. This finding indicates the occurrence of a superparamagnetic phase, which can be assigned to Fe atoms in Nd rich environments. These results indicate that the optimum deposition conditions correspond to 15 min ablation time for each of the two targets, which corresponds to a final film thickness of about 50 nm.

The XRD patterns were recorded for the  $\alpha$ -Fe/Nd<sub>2</sub>Fe<sub>14</sub>B multilayers after 15, 30 and 60 min of deposition from each target. Besides the lines coming from the silicon substrate, the spectra indicate the formation of the Nd<sub>2</sub>Fe<sub>14</sub>B phase. Again, the best structure corresponds to the film ablated for 15 min per target. We displayed the XRD spectra of the  $\alpha$ -Fe/Nd<sub>2</sub>Fe<sub>14</sub>B multilayers, obtained at 15, 30 and 60 min per target and subsequently exposed to thermal annealing at 550°C for 1 hour. The spectra were proven consistent with the formation of  $\alpha$ -Fe and Nd<sub>2</sub>Fe<sub>14</sub>B soft and hard phases, along with lines from Nd (which supports the occurrence of the superparamagnetic fraction) and hematite phases. An amorphous component, representing

the intermixing of phases, can be observed for the sample deposited for 1 hour per target. In agreement with the CEMS results, the best structure is formed at 15 min ablation time for each target.

#### IV. Cobalt-substituted spring magnets

We measured the XRD pattern of the  $\text{Nd}_{11}\text{Fe}_{80.6}\text{Co}_{2.6}\text{B}_{5.8}$  composition, annealed at 690 and 755°C. We could identify the soft phase  $\alpha\text{-Fe}(\text{Co})$ , which is crystalline and the hard phase  $\text{Nd}_2\text{Fe}_{14}\text{B}$ , which is predominantly amorphous. Similar features were exhibited by the samples  $\text{Nd}_{10.5}\text{Fe}_{78.4}\text{Co}_{5.3}\text{B}_{5.8}$  and  $\text{Nd}_{10}\text{Fe}_{76.5}\text{Co}_{7.9}\text{B}_{5.6}$  annealed at 690 and 775°C.

We also recorded the room temperature transmission Mössbauer spectra of the  $\text{Nd}_{11}\text{Fe}_{80.6}\text{Co}_{2.6}\text{B}_{5.8}$  system annealed at 690 and 755°C. We derived the hyperfine magnetic field distributions extracted from these spectra by nonlinear least-squares fitting (Figure 4). Similar spectra were obtained for the compositions  $\text{Nd}_{10.5}\text{Fe}_{78.4}\text{Co}_{5.3}\text{B}_{5.8}$  and  $\text{Nd}_{10}\text{Fe}_{76.5}\text{Co}_{7.9}\text{B}_{5.6}$  annealed at 690 and 775°C. In view of the XRD results, all Mössbauer spectra were analyzed with a six-line pattern corresponding to the  $\alpha\text{-Fe}(\text{Co})$  crystalline phase and a hyperfine magnetic field distribution representing the  $\text{Nd}_2\text{Fe}_{14}\text{B}$  amorphous component.

We obtained the dependence of the hyperfine magnetic field of the crystalline phase on the annealing temperature. It may be observed that the hyperfine magnetic field of the soft phase first increases with increasing Fe content and then increases with increasing the amount of Co substitution. Indeed, it is known that at certain compositions, Co has the tendency to increase the hyperfine fields at Fe sites and this effect prevails over that of increasing Fe content. The combined XRD and Mössbauer findings are consistent with the presence of Co substitutions in the soft magnetic phase.

We derived the dependence of the average hyperfine magnetic field of the hard,

amorphous phase as function of the annealing temperature for the  $\text{Nd}_{11}\text{Fe}_{80.6}\text{Co}_{2.6}\text{B}_{5.8}$ ,  $\text{Nd}_{10.5}\text{Fe}_{78.4}\text{Co}_{5.3}\text{B}_{5.8}$  and  $\text{Nd}_{10}\text{Fe}_{76.5}\text{Co}_{7.9}\text{B}_{5.6}$  systems. It was observed that the hyperfine magnetic field increased with increasing the Co content. In view of the ability of cobalt substitutions to increase the hyperfine field at Fe sites, this result is possible only if Co also enters the hard phase. Moreover, the hyperfine magnetic field slightly increases with increasing the annealing temperature of the compound.

[Fe/ Nd<sub>2</sub>Fe<sub>14</sub> B]

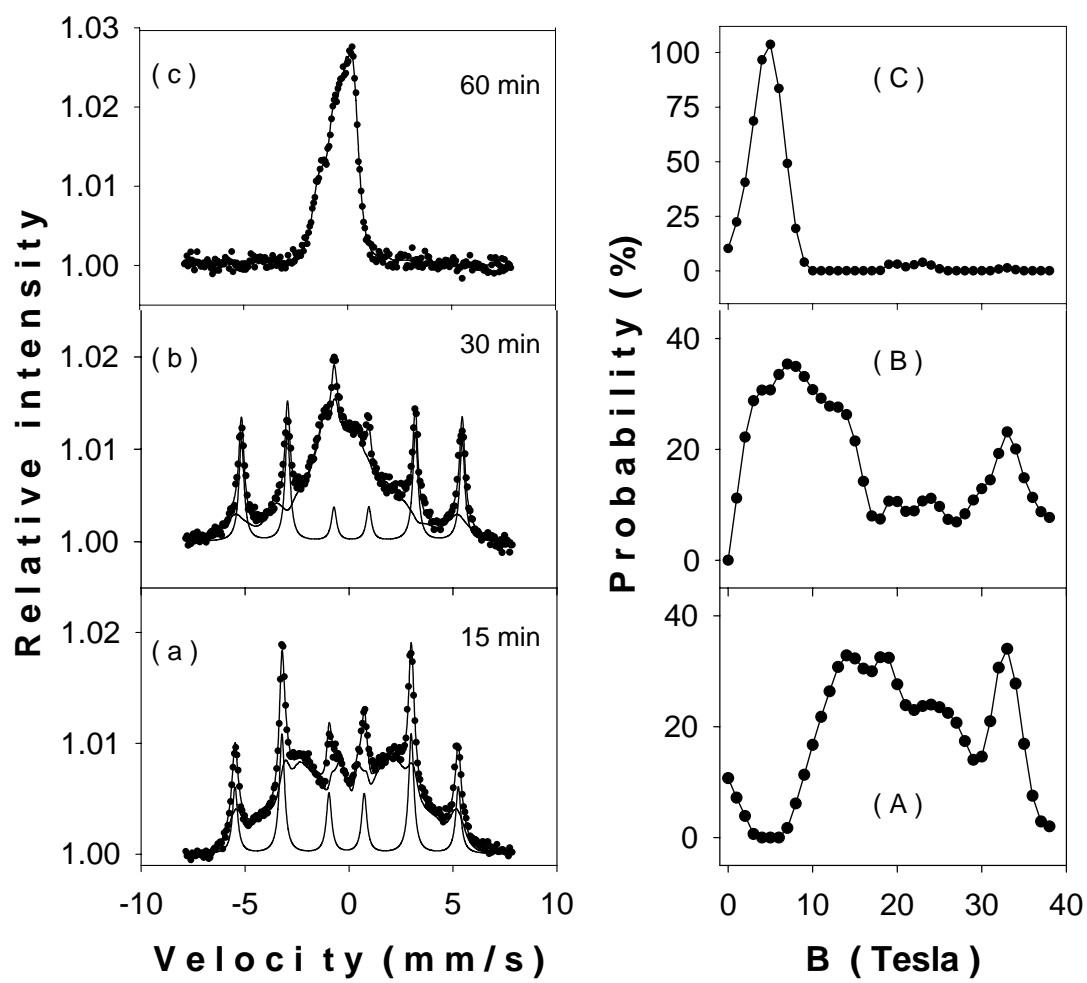
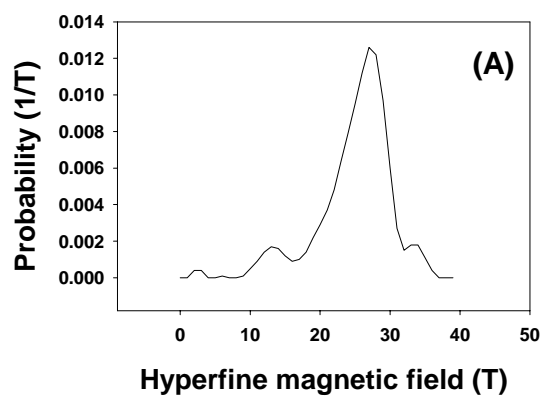
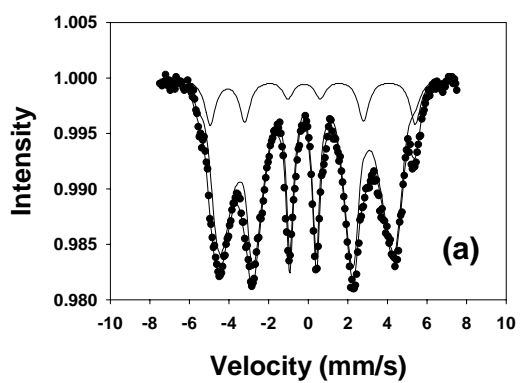


Figure 3

**Nd<sub>11</sub>Fe<sub>80.6</sub>Co<sub>2.6</sub>B<sub>5.8</sub>, 690 C**



**Nd<sub>11</sub>Fe<sub>80.6</sub>Co<sub>2.6</sub>B<sub>5.8</sub>, 755 C**

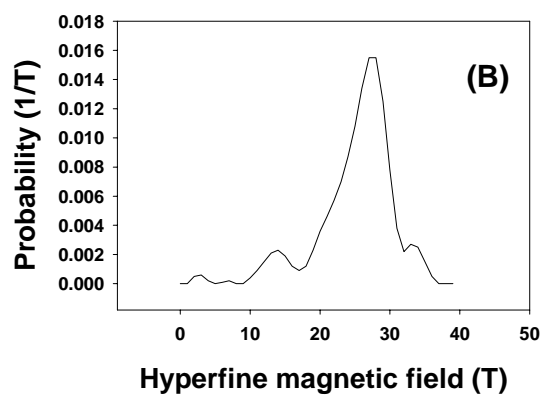
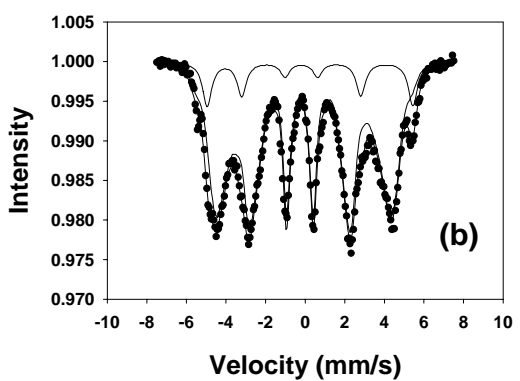


Figure 4

## CONCLUSIONS

We measured the recoilless fraction of the  $(1-x)\alpha\text{-Fe}_2\text{O}_3\text{-}x\text{SnO}_2$  nanoparticle system using the dual absorber method. The dependence of the recoilless fraction on the amount  $x$  of substitution showed that tin is a substitutional impurity in the hematite structure, and so is iron in the  $\text{SnO}_2$  lattice. The phase separation between  $\alpha\text{-Fe}_2\text{O}_3$  and  $\text{SnO}_2$  at  $x=0.4$  was observed as a minimum in the recoilless fraction. Particle size effects at large values of  $x$  were also evidenced.

$\alpha\text{-Fe}_2\text{O}_3\text{-In}_2\text{O}_3$  mixed oxide nanoparticles system has been synthesized starting with an aqueous solution of iron (III) nitrate nanohydrate and indium (III) nitrate pentahydrate, after 4 hours of hydrothermal supercritical synthesis at  $400^\circ\text{C}$  followed by one hour annealing at  $500^\circ\text{C}$ . It was found that a corundum phase  $\alpha\text{-(Fe}_{1-x}\text{In}_x)_2\text{O}_3$ , isostructural with  $\alpha\text{-Fe}_2\text{O}_3$  exists for  $0 < x \leq 0.9$  and a cubic phase  $c\text{-(Fe}_{1-x}\text{In}_x)_2\text{O}_3$ , isostructural with  $\text{In}_2\text{O}_3$  exists for  $0.3 \leq x < 1$ , in the nanoparticles system. The solid solutions phases,  $\alpha\text{-(Fe}_{1-x}\text{In}_x)_2\text{O}_3$ , and  $c\text{-(Fe}_{1-x}\text{In}_x)_2\text{O}_3$ , develop for indium nominal molar concentration  $x$  up to 0.7, and respectively for  $x$  from  $\approx 1.0$  to 0.7. The substitution level is generally up to 40% lower than the nominal concentration. An explanation of the processes leading to the formation of iron and indium phases (oxides and hydroxides) in the supercritical hydrothermal system  $(1-x)\text{Fe}(\text{NO}_3)_3 \cdot 9\text{H}_2\text{O} \cdot x\text{In}(\text{NO}_3)_3 \cdot 5\text{H}_2\text{O}$  has been given. This synthesis route allowed us to reach the nanometric particle dimensions and solid solutions in an extended concentration range, which would make them very attractive for sensing applications.

In conclusion,  $\alpha\text{-Fe}/\text{Nd}_2\text{Fe}_{14}\text{B}$  multilayer structures were obtained by pulsed laser deposition and characterized by CEMS and XRD. The optimum deposition conditions were identified and the structural and magnetic properties were examined for each sample.

It can be observed that the hyperfine magnetic field increases with increasing the Co content. In view of the ability of cobalt substitutions to increase the hyperfine field at Fe sites,

this result is possible only if Co also enters the hard phase. Moreover, the hyperfine magnetic field slightly increases with increasing the annealing temperature of the compound. To conclude, this study demonstrates that Co substitutions in spring magnets are present both in the soft and hard phases of the Nd-Fe-B exchange-coupled magnets.

## REFERENCES

1. W. Gopel, Sens. Actuators B 18-19 (1994) 1.
2. N. Yamazoe, N. Miura, Sens. Actuators B 20 (1994) 95.
3. J. Tamaki, C. Naruo, Y. Yamamoto, M. Matsuoka, Sens. Actuators B 83 (2002) 190.
4. J.Z Jiang, R. Liu, S. Morup, K. Nielsen, F.W. Poulsen, F.J. Berry and R. Clasen, Phys. Rev. B 55 (1997) 11.
5. J.Z. Jiang, R. Liu, K. Nielsen, S. Morup, K. Dam-Johansen and R. Clasen, J. Phys. D: Appl. Phys. 30 (1997) 1459.
6. W. Zhu, O.K. Tan and J.Z. Jiang, J. Mater. Electron. 9 (1998) 275.
7. O.K. Tan, W. Zhu, Q. Yan and L.B. Kong, Sens. Actuators B 65 (2000) 361.
8. C.V. Gopal Reddy, W. Cao, O.K. Tan and W. Zhu, Sens. Actuators B 81 (2002) 170.
9. M. Sorescu, L. Diamandescu, D. Tarabasanu-Mihaila, V.S. Teodorescu and B.H. Howard, J. Phys. Chem. Solids 65 (2004) 1021-1029.
10. M. Sorescu, Mater. Lett. 54 (2002) 256.
11. M. Sorescu, J. Nanopart. Res. 4 (2002) 221.
12. M. Sorescu, J. Mater. Sci. Lett. 21 (2002) 283.
13. M. Sorescu, J. Mater. Sci. Lett. 21 (2002) 1759.
14. J. Tamaki, C. Naruo, Y. Yamamoto and M. Matsuoka, Sens. Actuators B 83 (2002) 190.
15. F. Quaranta, R. Rella, P. Siciliano, A. Capone, C. Distante, M. Epifani, A. Taurino, Sens. Actuators B 84 (2002) 55.
16. O.K. Tan, W. Cao, W. Zhu, J.W. Chai, J.S. Pan, Sens. Actuators B 93 (2003) 396.
17. S.R. Kim, H.K. Hong, C.H. Kwon, D.H. Yun, K. Lee, Y.K. Sung, Sens. Actuators B 66 (2000) 59.



- 18.M. Marezio, Acta Cryst. 20 (1966) 723.
- 19.C.T. Prewitt, R.D. Shannon, D.B. Rogers and A.W. Sleight, Inorg. Chem. 8 (1969) 1985.
- 20.M. Ristić, S. Popović, M. Tonković, S. Musić, J. Mater. Sci. 26 (1991) 4225.
- 21.C.P. Udawate, K. Yanasigawa, J. Am. Ceram. Soc. 84 (2001) 251.
- 22.A. N. Christensen, N.C. Broch, O. Heidenstam, A. Nislon, Acta Chem. Scand. 21 (1967) 1046.
- 23.M. Sorescu, L. Diamandescu, D. Tarabasanu-Mihaila, V.S. Teodorescu, J. Mater. Sci. Lett., (2003), in press.
- 24.L. Diamandescu, D. Mihaila -Tarabasanu, M. Feder, Mat. Lett. 17 (1993) 309.
- 25.M.P. Morale, S. Veintemillas - Verdauger, C.J. Sema, J. Mater. Res. 14 (1999) 3066.
- 26.S. Music, I. Czako-Nagy, I. Salaj-Obelic, N. Ljubescic, Mat. Lett. 32 (1997) 301.
- 27.G. Ennas, G. Marangiu, A. Musinu, A. Falqui, P. Ballirano, R. Caminiti, J. Mater. Res. 14 (1999) 1570.
- 28.L. Diamandescu, D. Mihaila -Tarabasanu, N. Popescu-Pogrion, A. Totovana, I. Bibicu Ceram. Int. 25 (1999) 689.
- 29.R. Gerardin, A. Alebouyeh, O. Evrard, Mat. Res. Bull. 26 (1991) 455.
- 30.N.N. Greenwood, T.C. Gibb, *Mössbauer spectroscopy*, (Chapman and Hall Ltd., London 1971) p. 241.
- 31.*The Rietveld Method*, edited by R.A. Young (Oxford University Press, New York, 1993).
- 32.H.P. Klug and L.E. Alexander, *X-ray diffraction procedures for polycrystalline and amorphous materials*, (J. Wiley and Sons, New York, 1966) p. 491.
- 33.S. Musić, A. Vértes, G.W. Simmons, I. Czako-Nagy, H.Jr. Leidheiser, J. Coll. Interface Sci. 85 (1982) 256.
- 34.T. Adschiri, Y. Hakuta, K. Sue, K. Arai, J. Nanoparticle Res., 3 (2001) 227.

- 35.M. Sorescu, A. Grabias and M. Vaeleanu, IEEE Trans. Magn. 39 (2003) 2959
- 36.S. Steyaert, J.M. Le Breton, S. Parhofer, C. Kuhrt and J. Teillet, J. Magn. Magn. Mater. 196-197 (1999) 48
- 37.M. Shindo, M. Ishizone, H. Kato, T. Miyazaki and A. Sakuma, J. Magn. Magn. Mater. 161 (1996) L1
- 38.C. J. Yang and S.W. Kim, J. Magn. Magn. Mater. 202 (1999) 311
- 39.I. Panagiotopoulos and G.C. Hadjipanayis, Nanostruct. Mater. 10 (1998) 1013
- 40.E. Fullerton, J.S. Jiang and S.D. Bader, J. Magn. Magn. Mater. 200 (1999) 392
- 41.C.J. Yang, S.W. Kim and J.S. Kang, J. Magn. Magn. Mater. 188 (1998) 100
- 42.J. L. Tsai, T.S. Chin and J.C. Shih, IEEE Trans. Magn. 35 (1999) 3337
- 43.J.F. Herbst, J.J. Croat and F.E. Pinkerton, Phys. Rev. B 29 (1984) 4176
- 44.M. Sorescu, A. Grabias and M. Vaeleanu, Internet. 9 (2001) 67
- 45.M. Sorescu, A. Grabias and M. Vaeleanu, IEEE Trans. Magn. 39 (2003) 2959
- 46.E.F. Kneller and R. Hawig, IEEE Trans. Magn. 27 (1991) 3588
- 47.A. Manaf, R.A. Buckley and H.A. Davies, J. Magn. Magn. Mater. 128 (1993) 302
- 48.J. Bauer, M. Seeger, A. Zern and H. Kronmuller, J. Appl. Phys. 80 (1996) 1667
- 49.J. Ding, Y. Li and K.Y. Lee, J. Phys.: Condens. Matter 10 (1998) 9081
- 50.T. Kobayashi, M. Yamasaki and M. Hamano, J. Appl. Phys. 87 (2000) 6579
- 51.Y.Q. Wu, D.H. Ping, K. Hono, M. Hamano and A. Inoue, J. Appl. Phys. 87 (2000) 8658
- 52.H. Onodera, A. Fujita, H. Yamamoto, M. Sagawa and S.J. Hirose, J. Magn. Magn. Mater. 68 (1997) 6
- 53.Z.H. Cheng, G. Shen, M.X. Mao, J.J. Sun, Y.D. Zhang and F.S. Li, Phys. Rev. B 52 (1995) 9427
- 54.M.M. Raja and A. Narayanasami, J. Appl. Phys. 84 (1998) 5715

## LIST OF ACRONYMS AND ABBREVIATIONS

XRD=X-ray diffraction

CEMS=conversion electron Mössbauer spectroscopy

PLD=pulsed laser deposition

SEM=scanning electron microscopy

TEM=transmission electron microscopy

EDX=energy-dispersive X-ray analysis

## LIST OF PUBLICATIONS

- 1) **M. Sorescu**, L. Diamandescu, D. Tarabasanu-Mihaila, V.S. Teodorescu and B.H. Howard, “Hydrothermal Synthesis and Structural Characterization of  $(1-x)\alpha\text{-Fe}_2\text{O}_3\text{-xSnO}_2$  Nanoparticles”, **Journal of Physics and Chemistry of Solids** 65 (2004) 1021-1029.
- 2) **M. Sorescu**, F. Pourarian and R.A. Brand, “Mössbauer Study of Hydrogenation Effects in Iron-Rich Intermetallics”, **Journal of Materials Science Letters** 22 (2003) 1569-1572.
- 3) **M. Sorescu**, A. Grabias, L. Diamandescu and D. Tarabasanu-Mihaila, “Bulk Versus Surface Effects in Magnetic Thin Films Obtained by Pulsed Laser Deposition”, **Applied Surface Science**, 217 (2003) 233-238.
- 4) **M. Sorescu** and M. Valeanu, “Effect of Substitutions on the Hyperfine Magnetic Field in Nd-Based Intermetallics”, **Intermetallics** 11 (2003) 749-754.
- 5) **M. Sorescu**, F. Pourarian and R.A. Brand, “Mossbauer Study of Hydrogenation Effects in Iron-Rich Intermetallics”, **Journal of Materials Science Letters** 22 (2003) 1569-1572.
- 6) **M. Sorescu**, A. Grabias and M. Valeanu, “A Mössbauer Study of Spring Magnets”, **IEEE Transaction on Magnetics** 39 (2003) 2959-2961.
- 7) **M. Sorescu**, L. Diamandescu and A. Grabias, “Evolution of Phases During Mechanochemical Activation in Magnetite-Containing Systems”, **Materials Chemistry and Physics** 83 (2004) 354-360.
- 8) **M. Sorescu**, L. Diamandescu, D. Tarabasanu-Mihaila and V.S. Teodorescu, “Nanocrystalline Rhombohedral  $\text{In}_2\text{O}_3$  Synthesized by Hydrothermal and Postannealing Pathways”, **Journal of Materials Science** 39 (2004) 675-677.
- 9) **M. Sorescu**, L. Diamandescu, R. Peelamedu, R. Roy and P. Yadoji, “Structural and Magnetic Properties of NiZn Ferrites Prepared by Microwave Sintering”, **Journal of Magnetism and Magnetic Materials**, 279 (2004) 195-201.
- 10) **M. Sorescu**, L. Diamandescu, R.A. Brand and D. Tarabasanu-Mihaila, “Mössbauer Study of Manganese-Doped Magnetite Below the Verwey Transition”, **Materials Letters** 58 (2004) 885-888.
- 11) **M. Sorescu**, L. Diamandescu and D. Tarabasanu-Mihaila, “ $\alpha\text{-Fe}_2\text{O}_3\text{-In}_2\text{O}_3$  Mixed Oxide Nanoparticles Synthesized Under Hydrothermal Supercritical Conditions”, **Journal of Physics and Chemistry of Solids**, 65 (2004) 1719-1725.
- 12) **M. Sorescu**, L. Diamandescu and M. Valeanu, “Effect of Cobalt Substitutions in Spring Magnets”, **Journal of Materials Science Letters**, in press.

- 13) **M. Sorescu**, L. Diamandescu and A. Grabias, “Pulsed Laser Deposition of Nanocomposite  $\alpha$ -Fe/Nd<sub>2</sub>Fe<sub>14</sub>B Magnets”, **Journal of Materials Science Letters**, in press.
- 14) **M. Sorescu**, L. Diamandescu and D. Tarabasanu-Mihaila, “Recoilless Fraction of Tin-Doped Hematite Nanoparticles Obtained by Hydrothermal Synthesis”, **Materials Letters**, in press.
- 15) **M. Sorescu**, L. Diamandescu, R. Swaminathan, M.E. McHenry and M. Feder, “Structural and Magnetic Properties of NiZn and Zn Ferrite Thin Films Obtained by Laser Ablation Deposition”, **Journal of Applied Physics**, submitted.
- 16) **M. Sorescu**, C.Y. Um, M.E. McHenry and L. Diamandescu, “Thermal Behavior of Substituted FeCo-Based Metallic Glasses”, **Journal of Non-Crystalline Solids**, submitted.